Ultra-narrow-bandwidth deep-red electroluminescence based on green plant-derived carbon dots

Renjing Chen, Zhibin Wang, Tao Pang, Qian Teng, Chenhao Li, Naizhong Jiang, Song Zheng, Ruidan Zhang, Yuanhui Zheng, Daqin Chen*, Fanglong Yuan**

R. Chen, Dr. Z. Wang, N. Jiang, S. Zheng, Dr. R. Zhang, Prof. D. Chen

College of Physics and Energy, Fujian Normal University, Fujian Provincial Key Laboratory of Quantum Manipulation and New Energy Materials, Fuzhou, 350117, China

Prof. T. Pang

Huzhou Key Laboratory of Materials for Energy Conversion and Storage, College of Science, Huzhou University, Zhejiang, Huzhou 313000, China

Prof. Y. Zheng, Prof. D. Chen

Fujian Science & Technology Innovation Laboratory for Optoelectronic Information, Fuzhou, Fujian 350116, P. R. China

Prof. Y. Zheng

College of Chemistry, Fuzhou University, Fuzhou, Fujian 350116, China

Prof. D. Chen

This article has been accepted for publication and undergone full peer review but has not been through the copyediting, typesetting, pagination and proofreading process, which may lead to differences between this version and the Version of Record. Please cite this article as doi: 10.1002/adma.202302275.

Fujian Provincial Collaborative Innovation Center for Advanced High-Field Superconducting Materials and Engineering, Fuzhou, 350117, China

Fujian Provincial Engineering Technology Research Center of Solar Energy Conversion and Energy Storage, Fuzhou, 350117, China

Q. Teng, C.H. Li, Prof. F. Yuan

Key Laboratory of Theoretical & Computational Photochemistry of Ministry of Education, College of Chemistry, Beijing Normal University, Beijing, 100875, China

E-mail: zhibinwang@fjnu.edu.cn (Z. B. Wang); dqchen@fjnu.edu.cn (D. Q. Chen); flyuan@bnu.edu.cn (F. L. Yuan)

Abstract: Deep-red light-emitting diodes (DR-LEDs, >660 nm) with high color-purity and narrow-bandwidth emission are promising for full-color displays and solid-state lighting applications. Currently, the DR-LEDs are mainly based on conventional emitters such as organic materials and heavy-metal based quantum dots (QDs) and perovskites. However, the organic materials always suffer from the complicated synthesis, inferior color purity with full-width at half-maximum (FWHM) more than 40 nm and the QDs and perovskites still suffer from serious problems related to toxicity. Herein, we report the synthesis of efficient and high color-purity deep-red carbon dots (CDs) with a record narrow FWHM of 21 nm and a high quantum yield of more than 50% from readily available green plants. Moreover, an exciplex host is further established using a polymer and small molecular blend, which has been shown to be an efficient strategy for producing high color-purity monochrome emission from deep-red CDs via Förster energy transfer. The deep-red CD-LEDs displays high color-purity with Commission Internationale de l'Eclairage (CIE) coordinates of (0.692, 0.307). To the best of our knowledge, this is the first report of high color-purity CD-LEDs in the deep-red region, opening the door for the application of CDs in the development of high-resolution light-emitting display technologies.

Keywords: carbon dots, narrow-bandwidth emission, deep-red, light-emitting diodes, co-host strategy

Introduction

Light-emitting diodes (LEDs) fabricated based on luminescent materials that exhibit high color purity narrow-bandwidth emission are promising for full-color vivid displays. Deep-red LEDs (>660 nm), as an important light source, not only meet the requirements of next-generation vivid flat panel displays, but also play an essential role in some specific solid-state lighting, including night-vision technologies,[1] optical communication,[2] photodynamic therapy,[3] and horticultural lighting.[4] Currently, deep-red LEDs are mainly fabricated using conventional emitters, such as organic materials and heavy-metal based quantum dots (QDs) and perovskites. **Table 1** summarizes the key optical parameters of the currently available deep-red emitters for LEDs. The well-developed organic LEDs (OLEDs) usually show inferior color purity with full-width at half-maximum (FWHM) more than 40 nm. Color filters or optical microcavities are usually used to enhance the color purity of the original electroluminescence (EL) spectra of OLEDs, resulting in significant energy losses. In addition, the complicated material synthesis and device fabrication process further limits their wide practical applications. Colloidal QDs, typified by cadmium-based II-VI group semiconductors and metal halide perovskites, have drawn immense attention due to their exceptional properties, including high photoluminescence quantum yield (PLQY), narrow FWHM, broad spectral tunability, and cost-effective solution-processability.[5] Unfortunately, these high-performance deep-red LEDs must introduce highly toxic heavy metals (e.g., Cd^{2+}, Hg^{2+}, or Pb^{2+}), of which the content of these elements have been strictly restricted by the European Union and some countries, making it extremely tough for their practical applications and future commercialization.[6, 7] Therefore, the development of new generation of environmentally friendly, and low toxic light-emitting materials with excellent optical

properties for the next-generation high-performance full-colour display and lighting technologies is highly desired.[8]

Table 1. Key parameters of deep-red emitters for DR-LED devices.

Materials category	Example	Toxic	Emission peak (nm)	FWHM (nm)	CIE	Ref.
Cd-based NCs	CdS/CdZnS	Yes	667	30	(0.719, 0.278)	[6]
Perovskite QD solids	$CsPbI_3$	Yes	679	35[a)]	(0.73, 0.27)	[9]
Perovskite QDs	$CsPbI_3$	Yes	690	37	(0.721, 0.275)	[10]
Quasi-2D perovskite	$L_2CsPb_2I_7$	Yes	680	34	(0.722, 0.277)	[11]
Organic molecule	*t*BuTPA-CNQx	No	662	80[a)]	(0.67, 0.32)	[12]
Carbon dots	**DR-NBE-CDs**	**No**	**673**	**21**	**(0.721, 0.277)**	**This work**

[a)](These data were estimated from the figure in references).

In the last few years, carbon dots (CDs) as emerging emitters have attracted tremendous attention for electroluminescent LEDs due to the high photostability, easy synthesis, low toxicity, tunable light emission, and solution-processability. A variety of CDs with high PLQY have been

realized with the emissions ranging from blue to green, while CDs with high PLQY in the longer emission wavelength region especially in the deep-red region still remains a big challenge. Besides, most reported CDs show broadband emission spectra with a large FWHM (>80 nm), which is very unfavorable for efficient wide-color gamut displays.[13] Recently, bright deep-red carbonized polymer dots (CPDs) have been successfully synthesized by Yang's group, the as-prepared CPDs derived from taxus leaves achieved unprecedented narrow FWHM of only 20 nm, and were used for one-photon and two-photon bioimaging applications.[14] Xiong and their coworkers prepared bright deep-red emissive CDs made from mulberry leaves through solvothermal method.[15] More intriguingly, the as-synthesized CDs could be fed to silkworms safely to produce brightly fluorescent silk, indicating the good biocompatibility of these CDs. These nature biomass-derived CDs (e.g., coal,[16] fruit,[17] plant leaves,[18] and seeds[19]) have been used in optoelectronic and biological applications, which is expected to shine brightly in electrically driven light-emitting diodes.[20]

Recently, electrically driven CD-based LEDs (CD-LEDs) from deep-blue to red (420-630 nm) have been demonstrated (Table S1). However, the deep-red CD-LEDs (>660 nm), especially for those with high color purity and narrow emission bandwidth, have not yet been realized.[21] CD-LEDs usually suffer from the fluorescence quenching issue when neat CDs are used as the light-emitting layer due to the aggregation-induced quenching (AIQ) effect.[22, 23] To solve this problem, most CD-LEDs adopt the host-guest strategy, generally with poly(N-vinyl carbazole) (PVK), poly(9,9-dioctylfluorene-co-N-(4-(3-methylpropyl))diphenylamine) (TFB), and other host materials mixed with CDs.[22] The utilization of a host-guest strategy has been shown to effectively suppress the quenching of CDs in the solid film. However, the host material usually shows a large bandgap (>3 eV), much larger than that of the deep-red emission CDs (<1.9 eV), which thus lead to an insufficient energy transfer

process during the device operation. Therefore, the deep-red EL spectra are frequently accompanied by the presence of parasitic emission associated with the host materials, which cannot meet the requirements of high color purity displays. Thus, devising a more rational device architecture is a crucial determinant in realizing high color-purity deep-red CD-LEDs.

In this work, we report the synthesis of deep-red narrow-bandwidth emission CDs (DR-NBE-CDs) via a solvothermal method utilizing natural green plant as the carbon resource. The resulting DR-NBE-CDs displayed bright deep-red emission peaking at 673 nm with a narrow FWHM of 21 nm and a high PLQY of up to 52.35%. To suppress the AIQ effect and avoid the parasitic emission associated with the host materials for achieving efficient and high color-purity EL emission from DR-NBE-CDs, a blend of the polymer poly[bis(4-phenyl)(2,4,6-trimethylphenyl)amine] (PTAA) and the small molecular 2,4,6-tris[3-(diphenylphosphinyl)phenyl]-1,3,5-triazine (PO-T2T) were employed as a co-host to form an exciplex, which facilitates the efficient Förster energy transfer (FET) from the exciplex to DR-NBE-CDs. Consequently, the DR-NBE-CDs based device exhibited deep-red emission with Commission Internationale de l'Eclairage (CIE) coordinates of (0.692, 0.307). The CD-LED also presented remarkable performance with a maximum luminance (L_{max}) of more than 500 cd m^{-2}, providing new possibilities of low-cost and environmentally friendly CDs for high-color purity displays and specific lighting applications.

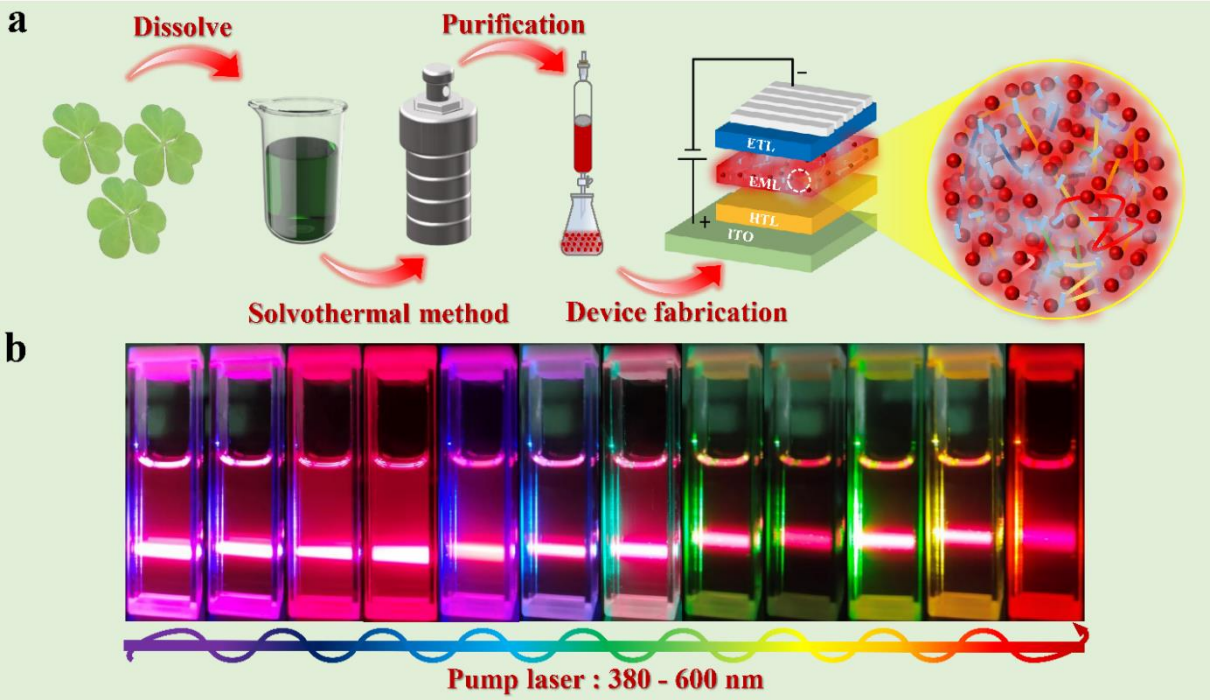

Figure 1. (a) Schematic diagram of the synthesis and application process of DR-NBE-CDs. (b) Photographs of fluorescent DR-NBE-CDs under femtosecond laser excitation.

Results and discussion

The synthesis of DR-NBE-CDs were performed using the solvothermal method and fresh clovers as the carbon resource, as depicted in **Figure 1a**. The process began with the grinding of the clovers using a food mincer, followed by extraction of the solution using ethanol. The precursor solution was then transferred into a Teflon-lined autoclave and subjected to solvothermal heating at 150°C for 6 h to yield the crude product. Afterward, the crude product was subsequently purified through silica column chromatography method to obtain the DR-NBE-CDs, which were dispersed in 1,2-dichlorobenzene (ODCB). As shown in **Figure 1b**, bright deep-red emissions from the DR-NBE-CDs

were observed under a range of femtosecond laser excitations (power density of 0.25 μJ/cm^2) from 380 to 600 nm, indicating that the fluorescence originates from a single radiative recombination center. The absolute PLQY of DR-NBE-CDs was estimated to be 52.35% under 400 nm excitation, which is among the highest reported PLQY values for deep-red CDs to date.[14, 15] The synthesis of DR-NBE-CDs can be scaled up using a 250 mL Teflon-lined autoclave. As shown in the **Figure S1a**, the crude DR-NBE-CDs display intense deep-red fluorescence when excited by UV light. Following purification via silica column chromatography and solvent evaporation, almost 0.59 g of purified DR-NBE-CDs were obtained, as indicated in **Figure S1b**.

In addition, we have chosen ten commonly found green plants and synthesized DR-NBE-CDs using the same method. The resulting DR-NBE-CDs exhibit comparable fluorescence spectra with QYs ranging from 12.43% to 52.35% (**Figure S2**). These findings indicate the universal potential of green plants for DR-NBE-CDs synthesis. In fact, the fluorescence origin of deep-red CDs derived from plants is still a topic of debate due to their complex structure. For example, Yang et al. synthesized bright deep-red carbonized polymer dots from taxus leaves, and they contributed the deep-red emission to the carbon cores consisting of aromatic rings and N heterocycles.[14] Liu et al. also ascribed the deep-red emission of mulberry-leaves-derived CDs to the highly graphitized conjugated system.[15] However, it is widely acknowledged that the narrow-band NIR emission of chlorophylls in green plants is attributed to their porphyrin structure. Thus, the origin of the deep-red emission could be related to the porphyrin molecular chromophores in chlorophylls. The UV-vis absorption and fluorescence spectra of the commercially available chlorophylls ab exhibit similarities to that of DR-NBE-CDs. Nonetheless, there are notable distinctions in the PLQY between the two materials (**Figure S3**). Therefore, we speculate that chlorophyll is the primary component extracted through

ethanol, but other components, such as flavonoids, polysaccharides, proteins, and lignin, may also contribute to the formation of DR-NBE-CDs.[14,15]

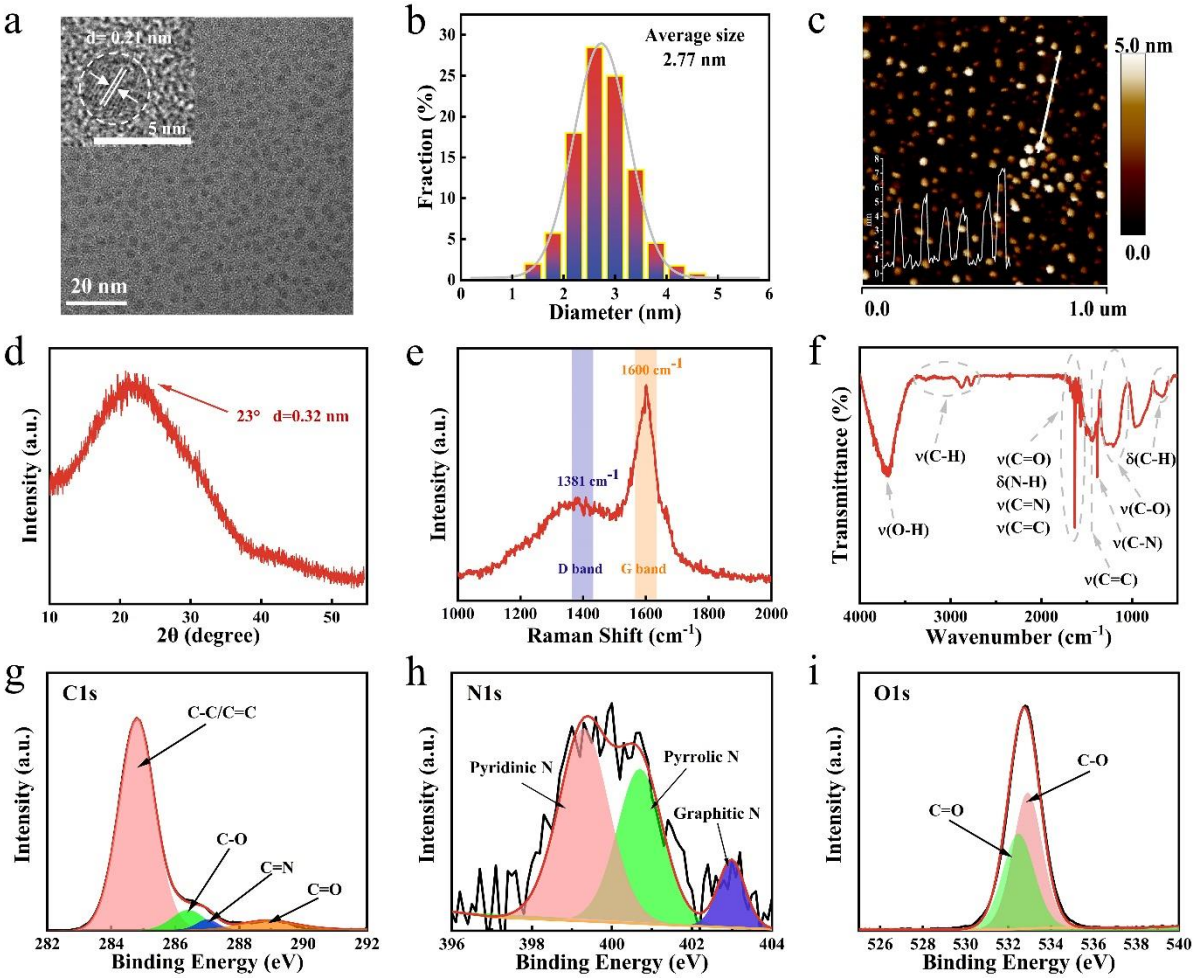

Figure 2. (a) TEM image of DR-NBE-CDs. Inset is HRTEM image. (b) Diameter histogram of the DR-NBE-CDs. (c) AFM image of the DR-NBE-CDs. Inset is the height profile of particles alone the white line in (c). (d) XRD pattern, (e) Raman spectra, (f) FT-IR spectrum of DR-NBE-CDs. High-resolution (g) C 1s, (h) N 1s, and (i) O 1s XPS spectra of DR-NBE-CDs.

The morphologies of DR-NBE-CDs were identified by transmission electron microscopy (TEM) and atomic force microscopy (AFM). TEM image reveals that the DR-NBE-CDs are nanodots that are distributed evenly (**Figure 2a**). The high-resolution TEM (HRTEM) image, shown in the inset, exhibits a lattice spacing of 0.21 nm, as estimated through fast Fourier transform (FFT) calculation, consistent with the in-plane (100) lattice spacing of graphene. (**Figure S4a**).[22, 24] As depicted in **Figure 2b,** the size distribution of DR-NBE-CDs was determined by counting approximately 400 particles (**Figure S4b**), which revealed a size distribution ranging from 1.5 to 4.8 nm, with an average size of 2.77 nm. The AFM topography image of DR-NBE-CDs showed an average size of 5.2 nm (**Figure 2c** and **Figure S5**). The difference in size between TEM and AFM is indicative of the core-shell structure of the carbonized polymer dots that make up the DR-NBE-CDs.[25] Given the low contrast of polymer chains in TEM testing, it is suggested that the actual sizes of DR-NBE-CDs should be based on the AFM results.[14] The DR-NBE-CDs show a broad diffraction peak at around 23° in the X-ray powder diffraction (XRD) pattern, as shown in **Figure 2d**, confirming the (002) lattice spacing of graphite structure and small size of the CDs.[26] The Raman spectrum of the DR-NBE-CDs features two peaks at 1381 and 1600 cm^{-1}, which correspond to the D band (representing the carbon associated with defects and disorder) and G band (representing the in-plane stretching vibration of the sp^2 domains), respectively (**Figure 2e**).[27] The intensity ratio of G band to the D band (I_G/I_D) is 1.85, which is comparable to other reported CDs.[28,29]

The chemical composition of DR-NBE-CDs were determined by Fourier transform infrared (FTIR) spectroscopy, as shown in **Figure 2f**. Characteristic peaks at 1630-1750 cm^{-1} were observed, corresponding to the stretching vibrations of C=C, C=O, and C=N, indicating the presence of aromatic rings and large conjugated systems. Additionally, DR-NBE-CDs showed peaks in the range of 2877-

3265 cm^{-1}, which corresponded to the vibrations of -CH_2-, indicating the existence of hydrophobic long alkyl chains on the surface of DR-NBE-CDs. Furthermore, the presence of a polymer shell consisting of alkyl chains was confirmed by the peaks observed at 600-768 cm^{-1}, which could be attributed to C-H out-of-plane bending vibrations. Additionally, a peak at 1387 cm^{-1} was observed, representing C-N stretching vibrations, while the characteristic peaks observed at 1046-1353 cm^{-1} corresponded to C-O-C of the ester group stretching vibrations, which could be associated with the ester group of chlorophyll.[30] Full X-ray photoelectron spectroscopy (XPS) spectrum of the DR-NBE-CDs revealed the presence of three primary elements: C (67.81%, atomic percentage), N (1.95%, atomic percentage), and O (30.24%, atomic percentage), as evidenced by the three typical C1s (284.8 eV), N 1s (399.3 eV), and O 1s (532.8 eV) (**Figure S6**). The deconvoluted high-resolution XPS curves of C1s (**Figure 2g**) comprised peaks of four different components, which corresponded to C=C/C-C (284.8 eV), C-O (286.4 eV), C=N (287 eV), and C=O (288.9 eV).[15] As shown in **Figure 2h**, the high-resolution N 1s band reveals pyridinic N (399.3 eV), pyrrolic N (400.7 eV), and graphitic N (402.9 eV), while the high-resolution O 1s band (**Figure2i**) could be deconvoluted into two peaks of C=O (532.5 eV) and C-O (532.9 eV).[30] The XPS results were consistent with the aforementioned FTIR analysis, thus further confirming the conclusion that the DR-NBE-CDs consist of external polymer chains that envelop a π-conjugated core.

To further identify the polymer characteristics of DR-NBE-CDs, we conducted thermogravimetric analysis (TGA) and derivative thermogravimetric analysis (DTG) measurements, as shown in **Figure S7**. The initial weight loss observed can be attributed to the evaporation of water molecules and the decomposition of light organic compounds.[30, 32] As the temperature was raised to above 200°C, an obvious decomposition process occurred with a peak thermal decomposition rate

at 255℃, indicating the decomposition of amides, esters, unsaturated double bonds, etc.[14] As the temperature is raised to 325℃, the polymer chains break and the degree of carbonization increases. The CDs obtained at higher reaction temperatures (220℃and 280℃) confirm the destruction of molecular fluorophores (**Figure S8**). Therefore, the deep-red emission originates from the fluorescent molecular centers rather than the carbon cores.

We conducted measurements of ^{1}H and ^{13}C nuclear magnetic resonance (NMR) spectra of CDs to gain further insights into the fluorescent molecular structure responsible for the deep-red emission (**Figure S9**). The ^{1}H NMR spectrum reveals obvious signals in the 2.0-4.5 ppm and 6.0-9.0 ppm ranges, the former correspond to nitrogen heterocyclic H, while the latter represent the pyrrole H, aromatic H, and pyridine H, respectively.[14, 33] These signals are possibly associated with the porphin structure in the DR-NBE-CDs. In the ^{13}C NMR spectrum, signals within the range of 13-33 ppm are in agreement with those observed in the ^{1}H NMR spectrum in the 0.7-1.9 ppm range, which are assigned to the alkyl chain stem from phytol possibly associated with chlorophylls. Additionally, signals in the 120-140 ppm range are indicative of the sp^2 C atoms, while signals in the 170-180 ppm range correspond to carboxyl groups. However, due to the extremely complex structure of CDs, precise structural characterization remains a major challenge, more efforts and advanced characterizations are needed.

As discussed above, it should be noted that the deep-red emission originates from the fluorescent molecular centers within the CDs, rather than being attributed to individual small organic molecules. Through multiple rounds of silica column chromatography separation and purification, we were able to isolate the deep-red emission component, which TEM and AFM analysis revealed to be nanodots rather than small organic molecules. Therefore, the deep-red

emission component is not merely mixed with CDs but is an integral part of the CDs themselves, and cannot be separated from the carbon core. During the thermal conditions, chlorophyll molecules undergo polymerization and carbonization to generate CDs while retaining the emission properties of the molecular chromophores.[34] The CDs synthesized through this polymerization and carbonization route exhibit higher fluorescence efficiency and thermal stability, attributed to cross-linking-induced emission enhancement.[25, 35] As depicted in **Figure S10**, it was not possible to obtain DR-NBE-CDs using pure chlorophyll as the precursor under the same reaction conditions. The molecular structure of chlorophyll was observed to undergo complete transformation into blue emission at 160℃, likely attributed to the breakdown of chlorophyll structures at elevated temperatures, as recently shown by Qin et al.[30] The researchers suspected that the biological microenvironment within plants may protect the luminescent center of chlorophyll during solvothermal treatment.

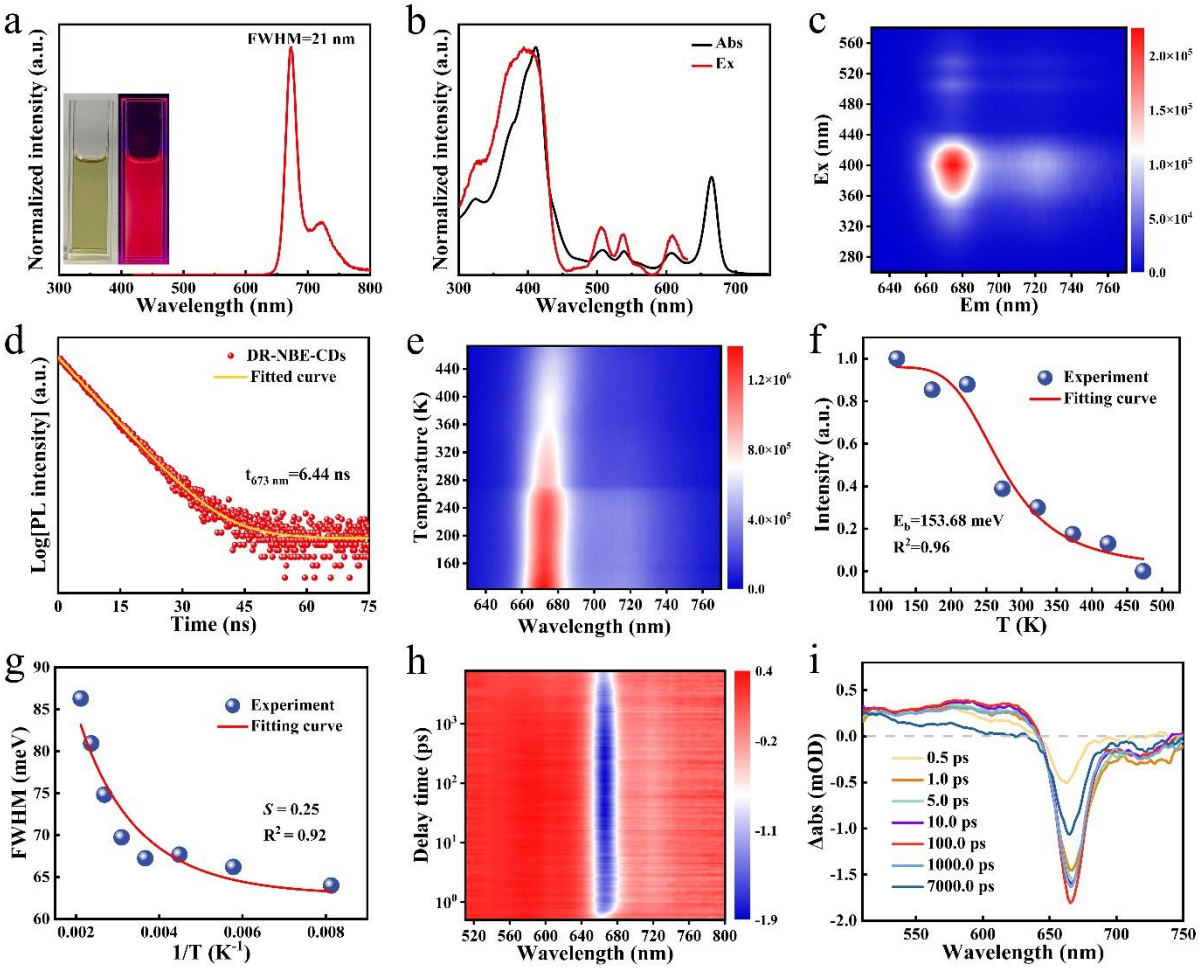

Figure 3. (a) PL spectra of DR-NBE-CDs solution excited at 400 nm. Inset: photographs of DR-NBE-CDs alcohol solution under daylight (left) and UV light (right), respectively. (b) The UV-visible absorption and excitation spectra of DR-NBE-CDs. (c) Two-dimensional excitation-emission mapping of the DR-NBE-CDs. (d) The PL decay curves of DR-NBE-CDs at 673 nm with an excitation wavelength of 375 nm. (e) Temperature-dependent PL spectra ranging from 123 to 473 K. (f) Fitting result of integrated PL intensity as a function of temperature. (g) Fitting result of FWHM as a function of temperature. (h) Two-dimensional pseudocolor map of transient absorption (TA) spectra of DR-NBE-CDs. (i) TA spectra of DR-NBE-CDs with different delay times from 0.5 ps to 7 ns.

The optical properties of DR-NBE-CDs in ethanol solution were investigated by UV-vis absorption and fluorescence spectra. The DR-NBE-CDs solution appears to be light-green under room light and exhibits intense deep-red emission upon ultraviolet (UV) excitation (365 nm, inset in **Figure 3a**). The DR-NBE-CDs exhibit a broad absorption band that extends from the UV to the deep-red region, as well as a sharp PL peak centered at 673 nm with a shoulder peak at 723 nm. The shoulder peak at longer wavelengths is ascribed to the inter-ring or intra-ring stretch modes of C-C, which are commonly observed in polyaromatic systems.[31] The absorption and excitation spectra of DR-NBE-CDs are virtually identical, with the optimal excitation wavelength around 400 nm (**Figure 3b**). Additionally, the DR-NBE-CDs display an ultra-small Stokes shift of 8 nm, indicating the band-edge exciton-state recombination and weak electron-phonon coupling interaction.[32] The dilute DR-NBE-CDs solution exhibit a high PLQY of 52.35% and an ultra-narrow FWHM of 21 nm (**Figure S11**), which is much narrower than that of organic materials, and even narrower than conventional Cd^{2+}- and Pb^{2+}-based QDs in the deep-red region.[33] The two-dimensional emission-excitation mapping of the DR-NBE-CDs solution (**Figure 3c**) exhibits a typical excitation-independent emission wavelength that remains constant over the range of 250-595 nm (measured at 15 nm intervals). As depicted in **Figure 3d**, the time-resolved PL spectrum of DR-NBE-CDs displays a mono-exponential decay with an average lifetime of 6.44 ns at the peak position of 673 nm, suggesting fast exciton recombination and minimal non-radiative recombination. To further evaluate the intrinsic properties of the photogenerated excitons in DR-NBE-CDs, we plotted a two-dimensional pseudocolor map of temperature-dependent PL spectra (**Figure 3e**). With elevation of temperature from 123 to 473 K, the thermal quenching of integrated PL intensity was found to be minimal, which suggests the high

thermostability of photogenerated excitons and the absence of significant non-radiative recombination centers in DR-NBE-CDs. The corresponding exciton binding energy was then extracted by plotting the integrated area of the PL emission intensity as a function of temperature according to the following equation:

$$I(T) = \frac{I_0}{1 + A\exp(\frac{-E_b}{k_b T})}$$

where I_0 represents the integrated intensity of the PL emission at 0 K, A is the proportional constant, E_b is the exciton binding energy, and k_b is the Boltzmann constant.[34] As illustrated in **Figure 3f**, the results of the fitting analysis demonstrate that DR-NBE-CDs possess a relatively large E_b of 153.68 meV, which is significantly higher than that of the previous reported CDs.[29,35] The radiative recombination rate was estimated based on the PLQY and the average lifetime of DR-NBE-CDs, yielding a value of 8.1×10^7 s^{-1} which is even fast than that reported for deep-red perovskite quantum dots.[36] The high E_b and fast radiative rate indicate an exceptional luminescent performance for DR-NBE-CDs.

The emission bandwidth of CDs is believed to be closely related to the strength of electron-phonon coupling. To determine this strength, the Huang-Rhys factor (S) is introduced as a measure, which can be classified into three regimes, weak coupling (S<1), intermediate coupling (1<S<5), and strong coupling (S>5). The S factor was estimated by plotting the FWHM as a function of the inverse temperature and fitting it using the following equation:

$$FWHM(T) = 2.36\sqrt{S}\hbar\omega_{photon}\sqrt{\coth\frac{\hbar\omega_{photon}}{2k_b T}}$$

where S is the Huang-Rhys factor and ω_{phonon} is the phonon frequency.[37] The S and ω_{phonon} are estimated to be 0.25 and 53 meV, respectively (**Figure 3g**). The small S value confirms the weak coupling between electronic transitions and lattice phonons in the DR-NBE-CDs. The results of the PL spectra analysis indicate that the FWHM values are ultra-narrow and that the bandwidth continuously narrows from 86.29 to 63.98 meV as the temperature decreases from 473 to 123 K. In the high temperature range, between 323 K and 473 K, the emission peak energy undergoes a blue-shift and the corresponding FWHM becomes narrower as the temperature goes down due to the suppression of molecular vibrations and distortions. Conversely, in the low temperature range between 123 K and 303 K, the PL position remains relatively unchanged, suggesting a relatively weak electron-phonon interaction. Based on these results, it can be inferred that the DR-NBE-CDs exhibit high structural rigidity and weak electron-phonon interaction, which may contribute to their ultra-narrow emission bandwidth.

To further understand the transfer and recombination dynamics of excitons in the femtosecond to nanosecond time domain, we performed femtosecond transient absorption (fs-TA) measurements of DR-NBE-CDs under a pump laser at 360 nm. As depicted in **Figure 3h**, we plotted the two-dimensional pseudo-color map of the transient TA spectra in the detection range of 510 to 800 nm, with scan delay times from 0.1 ps to 7.8 ns. The relatively weak positive (red) features from 510 to 640 nm correspond to the excited state absorption (ESA) signal, and the strong negative (dark blue) features from 645 to 750 nm correspond to the ground state bleaching (GSB) and stimulated emission (SE), agree well with the corresponding steady-state absorption and PL spectra. The TA spectra at different delay times (**Figure 3i**) demonstrate a gradual increase in the signal centered at 666 nm within 100 ps. This state-filling time of electrons and holes is consistent with the previously

reported results.[12] In addition, we performed energy gap calculations for DR-NBE-CDs by ultraviolet photoelectron spectroscopy (UPS) to determine the highest occupied molecular orbital (HOMO) and the lowest unoccupied molecular orbital (LUMO). As shown in **Figure S12**, the secondary electron cutoff (SEC) is estimated to be 18.18 eV and the HOMO region respect to the Fermi energy level was found to be 1.76 eV. Therefore, the value of HOMO was calculated as (21.22 eV-(18.18-1.76) eV) = 4.80 eV, where 21.22 eV is the energy of the photon source (He). The value of LUMO was determined as (4.80 eV-1.82 eV) = 2.98 eV, where 1.82 eV is the optical bandgap energy of DR-NBE-CDs (**Figure S13**).

The fluorescence efficiency of red-emitting CDs is often hindered by the strong π-π interaction between the large conjugated sp^2 domains in the aggregated state. To mitigate the AIQ in solid-state CDs, most reported CD-LEDs employ a host-guest emissive layer system. However, in the present work, a co-host system was established by utilizing a blend of PTAA and PO-T2T, instead of relying on pure PVK as the host. PTAA, as a hole transporting material, exhibiting a much higher hole mobility (1×10^{-3} cm^2 V^{-1} s^{-1}) compared to that of PVK (3×10^{-6} cm^2 V^{-1} s^{-1}), which enhances hole injection and transportation.[38] In the other hand, the electron-acceptor PO-T2T, which exhibits a high electron mobility (≈$1.7\text{-}4.4 \times 10^{-3}$ cm^2 V^{-1} s^{-1}), was introduced to balance the charge carrier by suppressing the over-injection of holes.[39] Both of these hosts have good solubility in aromatic solvents and can be solution-processed along with the DR-NBE-CDs through solution spin-coating method.

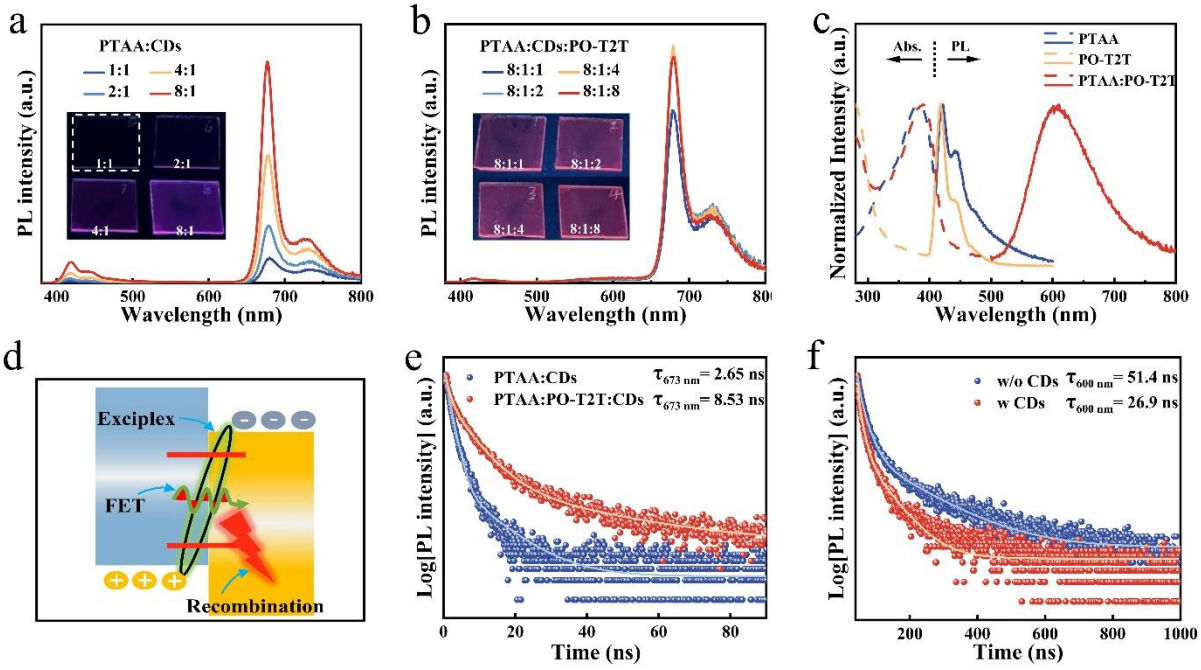

Figure 4. (a) PL spectra of PTAA:DR-NBE-CDs films. Insets are the corresponding photos under UV light irradiation. (b) PL spectra of PTAA:DR-NBE-CDs:PO-T2T films. Insets are the corresponding photos under UV light irradiation. (c) UV-vis absorption and PL spectra of PTAA, PO-T2T, and PTAA:PO-T2T in solid film. (d) Schematic diagram of Förster energy transfer process from exciplex to DR-NBE-CDs. (e) Time-resolved PL spectra of PTAA:DR-NBE-CDs and PTAA:DR-NBE-CDs:PO-T2T thin films at a probe peak of 673 nm. (f) Time-resolved PL spectra of PTAA:PO-T2T and PTAA:PO-T2T:DR-NBE-CDs thin films at a probe peak of 600 nm.

We fabricated emissive layers using PTAA as the host and DR-NBE-CDs as the guest, with the doping concentration controlled by adjusting the mixed volume ratios of PTAA and DR-NBE-CDs solutions (see detail in Experimental Section). As shown in **Figure 4a**, the PL intensity of CDs increased continuously with the increasing loading fraction of PTAA, which indicated that PTAA could

effectively suppress the AIQ of DR-NBE-CDs. Unfortunately, as the host ratio increased, blue parasitic emission from PTAA emerged, which suggested an incomplete energy transfer process. The corresponding photographs of PTAA:DR-NBE-CDs films exhibited a transition from non-luminous to purplish red, which was consistent with the results. To achieve pure DR-NBE-CDs emission, a more efficient FET process from organic host to CD guest was required. By employing a co-host system of PTAA:PO-T2T, the blue parasitic emission was notably quenched, and a dim new parasitic emission around 600 nm was observed (**Figure 4b**). The photographs of PTAA:PO-T2T:DR-NBE-CDs films confirm the more pure red emission. The UV-vis absorption and PL spectra of PTAA, PO-T2T, and PTAA:PO-T2T in solid film were also recorded (**Figure 4c**). The absorption spectrum of the PTAA:PO-T2T film can be expressed as linear combinations of the individual constituents, which implies that no new ground state complex formation or aggregation occurs. This observation suggests that the broad band emission at 600 nm is attributed to the exciplex.[40] Due to the high charge mobility and suitable energy levels of electron-donor (PTAA) and electron-acceptor (PO-T2T), holes and electrons were injected from and accumulated at the HOMO of the PTAA and the LUMO of PO-T2T, respectively, and thus excitons were formed. The excitons underwent radiative recombination to generate broad-band exciplex emission at ~600 nm.[41] The DR-NBE-CDs have a broad absorption band range from UV to deep-red region, which is well-overlapped with the PL spectra of neat PTAA or the exciplex of co-host. In the Förster energy transfer mechanism, a prerequisite of efficient energy transfer depends on the overlap between the emission spectrum of the host and the absorption spectrum of the guest.[42] Thus, the emission mechanism of DR-NBE-CDs can be ascribed to Förster energy transfer from exciplex host to DR-NBE-CDs guest, as illustrated in **Figure 4d**. The results indicated that the exciplex host retains better luminescent properties of DR-NBE-CDs than

the neat PTAA host. To determine the energy transfer efficiency from host to CDs, the PL decay behaviors were analyzed at a probe wavelength of 673 nm, as shown in **Figure 4e**. Results showed that the decay time of PTAA:DR-NBE-CDs was 2.65 ns, much shorter than that of the co-host:DR-NBE-CDs (8.53 ns), indicating a significant increase in Förster energy transfer from the exciplex host to the CDs guest. Additionally, the excited state lifetimes of the exciplex decreased from 51.4 to 26.9 ns after the introduction of DR-NBE-CDs, further confirmed the energy transfer process (**Figure 4f**). It should be noted that the lifetime of the neat PTAA host was only 1.81 ns (**Figure S14**), and we speculated that the incomplete Förster energy transfer was mainly due to the over-short excited state lifetime of the PTAA host.

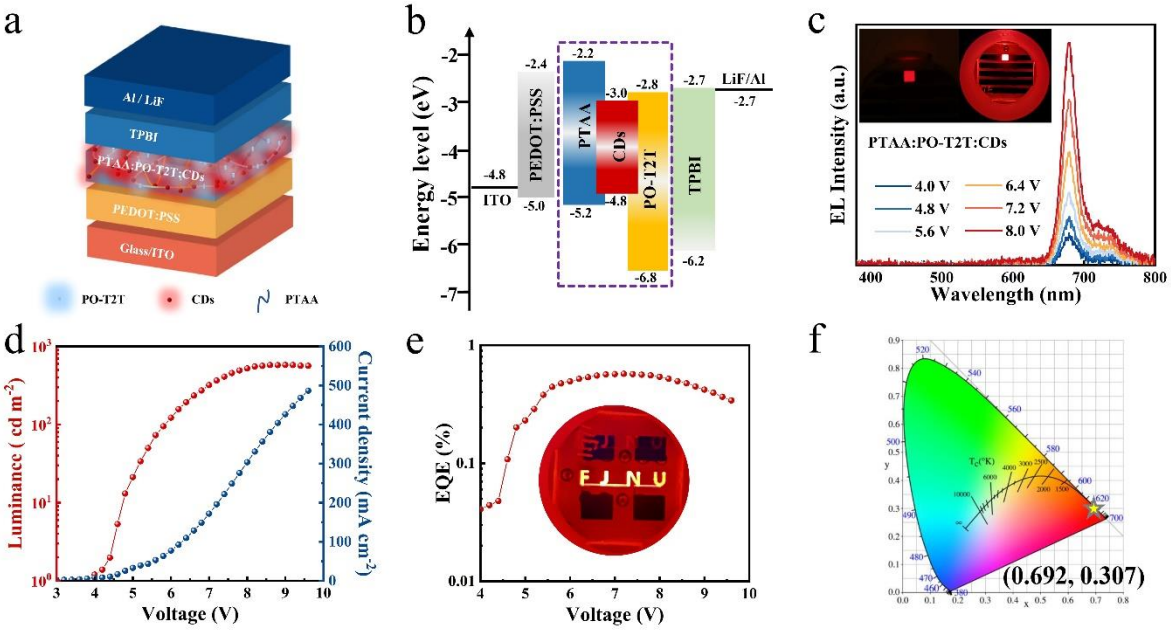

Figure 5. (a) Schematic illustration of the device architecture based on PTAA:PO-T2T:CDs as emissive layer. (b) The energy level diagram of DR-NBE-CDs-based LEDs. (c) EL spectra at different voltages. Inset: corresponding photograph of DR-NBE-CDs-based LEDs under constant voltage. (d) luminance-voltage-

current density (*L-V-J*) curve. (e) EQE-voltage curves. (f) The CIE coordinates of the DR-NBE-CDs-based LEDs.

To assess the effectiveness of utilizing exciplex as a strategy for producing deep-red CD-LEDs, a conventional device architecture was constructed. The architecture consists of an ITO anode, a hole injection layer of poly(2,3-dihydrothieno-1,4-dioxin)-poly(styrene sulfonate) (PEDOT:PSS), an emissive layer blended with PTAA:PO-T2T:DR-NBE-CDs, an electron transport layer of 1,3,5-tris(2-N-phenylbenzimidazolyl)-benzene (TPBi), and a LiF modified Al cathode, as depicted in **Figure 5a**. A diagram of the energy levels can be found in **Figure 5b**, where the HOMO and LUMO energy levels are situated within the HOMO of PTAA and LUMO of PO-T2T, respectively, which reduces the injection barriers and enhances the injection level of charge carriers. Hole- and electron-only devices (**Figure S15**) further demonstrate the balance of charge carrier injection. The use of electron-acceptor PO-T2T in comparison to the neat PTAA host led to reduced hole transport ability and enhanced electron transport ability, resulting in a more balanced charge carrier injection in the emissive layer. The EL spectra of the CD-LEDs based on neat PTAA and PTAA:PO-T2T hosts are presented in **Figure S16a** and **Figure 5c**, respectively. The CD-LEDs based on neat PTAA host displayed two EL peaks located at 420 and 676 nm, respectively. The blue emission was derived from the PTAA host, indicating incomplete energy transfer from host to guest. The corresponding luminance-voltage-current density (*L-V-J*) and EQE-voltage curves are displayed in **Figure S16b** and **S16c**. Similarly, when PVK was employed as the host material, the poor conductivity of PVK led to high injection barriers, and the large energy gap between PVK and CDs resulted in parasitic emission, ultimately impacting the device's overall performance (**Figure S17**). In contrast, the CD-LED based on

exciplex host exhibited a high-purity deep-red emission centered at 679 nm with an ultra-narrow FWHM of 25 nm under various applied bias, indicating efficient energy transfer from the exciplex host to CDs. The two insets demonstrate uniform and defect-free deep-red emission from the co-host-based CD-LEDs at low and high brightness, respectively. The corresponding luminance-voltage-current density (*L-V-J*) and EQE-voltage curves are shown in **Figure 5d** and **5e**, respectively. The CD-LED device based on PTAA:PO-T2T host shows a maximum brightness of 579 cd m^{-2} with a maximum EQE of 0.57%. Although the DR-NBE-CDs solution exhibits a high PLQY of 52.35%, the value decreases to 12.32% in the solid-state thin film (**Figure S18**). The fluorescence quenching of CDs in the solid state is a crucial factor that limits the improvement of device efficiency. In the future, finding ways to avoid the emission quenching and enhance the PLQY of CDs in the solid state will be crucial to boosting device performance. Additionally, achieving triplet emission of CDs and optimizing device structure will also be essential for improving device performance.

The photograph of CD-LED with the logo of Fujian Normal University (FJNU) displays bright and uniform red EL emission derived from DR-NBE-CDs. To the best of our knowledge, this is the first demonstration of deep-red electroluminescent CD-LEDs, which displayed an ultra-narrow FWHM of only 25 nm. As shown in **Figure 5f**, the corresponding coordinates of DR-NBE-CDs-based LEDs were calculated to be (0.692, 0.307), revealing extraordinary color purity of our device in the red region. The operational stability of the device was evaluated in a N_2-filled glove box without encapsulation, with an initial luminance of ~100 cd m^{-2}. The resulting operational lifetime T_{50} was 63 minutes (**Figure S19**). The peak luminance and EQE histograms for 48 devices displayed an average luminance of 461 cd m^{-2} and an average EQE of 0.49%, respectively. These outcomes provide evidence for the good reproducibility of the DR-NBE-CDs-based LEDs. (**Figure S20**).

Conclusion

In summary, we have introduced a widely available natural green plant as a precursor to synthesis bright deep-red CDs with a high PLQY of 52.35% and an ultra-narrow emission bandwidth of 21 nm. The morphometric and chemical composition analyses have revealed that the DR-NBE-CDs are composed of external polymer chains wrapping on the π-conjugated core. The optical properties analysis reveals that the ultra-narrow emission bandwidth of DR-NBE-CDs could be attributed to their high structural rigidity and weak electron-phonon interaction. To suppress the AIQ effect and enhance device performance, we have employed an exciplex host strategy for the first time in CD-LEDs. This strategy has successfully enabled the realization of high-performance monochrome deep-red emission through device structure engineering. The optimized CD-LEDs have exhibited high-purity deep-red emission centered at 679 nm with CIE coordinates of (0.692, 0.307), a maximum brightness of 579 cd m^{-2}, and a maximum EQE of 0.57%. This work not only provides a novel exciplex host strategy for achieving high-performance CD-LEDs, but also represents a significant breakthrough for the development of next-generation vivid flat panel display technologies that require monochrome CD-LEDs.

Supporting Information

Supporting Information is available from the Wiley Online Library or from the author.

***Corresponding Author**

E-Mail: zhibinwang@fjnu.edu.cn (Z. B. Wang); dqchen@fjnu.edu.cn (D. Q. Chen); flyuan@bnu.edu.cn (F. L. Yuan)

Declaration of Competing Interest

The authors declare no competing financial interests.

Acknowledgements

This research was supported by the National Natural Science Foundation of China (52102159, 52272141, 51972060, 12074068, and 22103013), Fujian Science & Technology Innovation Laboratory for Optoelectronic Information (2021ZZ126), the Natural Science Foundation of Fujian Province (2021J01187, 2020J02017, 2021J06021, 2021J01184, and 2020J01931), and special funds for introducing talents from Beijing Normal University (111032315).

Received: ((will be filled in by the editorial staff))
Revised: ((will be filled in by the editorial staff))
Published online: ((will be filled in by the editorial staff))

REFERENCES

[1] K. Tuong Ly, R.-W. Chen-Cheng, H.-W. Lin, Y.-J. Shiau, S.-H. Liu, P.-T. Chou, C.-S. Tsao, Y.-C. Huang, Y. Chi, *Nat. Photonics* **2017**, *11*, 63.

[2] A. Ren, H. Wang, W. Zhang, J. Wu, Z. Wang, R. V. Penty, I. H. White, *Nat. Electron.* **2021**, *4*, 559.

[3] C. Li, G. Chen, Y. Zhang, F. Wu, Q. Wang, *J. Am. Chem. Soc.* **2020**, *142*, 14789.

[4] Z. Kang, S. Wang, T. Seto, Y. Wang, *Adv. Opt. Mater.* **2021**, *9*, 2101173.

[5] a) Q. Lin, B. Song, H. Wang, F. Zhang, F. Chen, L. Wang, L. S. Li, F. Guo, H. Shen, *J. Mater. Chem. C* **2016**, *4*, 7223; b) T.-H. Han, K. Y. Jang, Y. Dong, R. H. Friend, E. H. Sargent, T.-W. Lee, *Nat. Rev. Mater.* **2022**, *7*, 757.

[6] S. Hu, F. Shabani, B. Liu, L. Zhang, M. Guo, G. Lu, Z. Zhou, J. Wang, J. C. Huang, Y. Min, Q. Xue, H. V. Demir, C. Liu, *ACS Nano* **2022**, *16*, 10840.

[7] a) V. Sayevich, Z. L. Robinson, Y. Kim, O. V. Kozlov, H. Jung, T. Nakotte, Y.-S. Park, V. I. Klimov, *Nat. Nanotechnol.* **2021**, *16*, 673; b) P. Sinha, C. J. Kriegner, W. A. Schew, S. W. Kaczmar, M. Traister, D. J. Wilson, *Energy Policy* **2008**, *36*, 381.

[8] Z. Zhang, *Nat. Rev. Mater.* **2022**, *7*, 839.

[9] Y. Jiang, C. Sun, J. Xu, S. Li, M. Cui, X. Fu, Y. Liu, Y. Liu, H. Wan, K. Wei, T. Zhou, W. Zhang, Y. Yang, J. Yang, C. Qin, S. Gao, J. Pan, Y. Liu, S. Hoogland, E. H. Sargent, J. Chen, M. Yuan, *Nature* **2022**, *612*, 679.

[10] H. Li, H. Lin, D. Ouyang, C. Yao, C. Li, J. Sun, Y. Song, Y. Wang, Y. Yan, Y. Wang, Q. Dong, W. C. H. Choy, *Adv. Mater.* **2021**, *33*, 2008820.

[11] J. Jiang, Z. Chu, Z. Yin, J. Li, Y. Yang, J. Chen, J. Wu, J. You, X. Zhang, *Adv. Mater.* **2022**, *34*, 2204460.

[12] S. Kothavale, S. C. Kim, K. Cheong, S. Zeng, Y. Wang, J. Y. Lee, *Adv. Mater.*, DOI: 10.1002/adma.202208602.

[13] B. Zhao, H. Ma, M. Zheng, K. Xu, C. Zou, S. Qu, Z. Tan, *Carbon Energy* **2022**, *4*, 88.

[14] J. Liu, Y. Geng, D. Li, H. Yao, Z. Huo, Y. Li, K. Zhang, S. Zhu, H. Wei, W. Xu, J. Jiang, B. Yang, *Adv. Mater.* **2020**, *32*, 1906641.

[15] J. Liu, T. Kong, H.-M. Xiong, *Adv. Mater.* **2022**, *34*, 2200152.

[16] C. Hu, C. Yu, M. Li, X. Wang, J. Yang, Z. Zhao, A. Eychmüller, Y.-P. Sun, J. Qiu, *Small* **2014**, *10*, 4926.

[17] G. Wang, Q. Guo, D. Chen, Z. Liu, X. Zheng, A. Xu, S. Yang, G. Ding, *ACS Appl.Mater. Interfaces* **2018**, *10*, 5750.

[18] L. Li, R. Zhang, C. Lu, J. Sun, L. Wang, B. Qu, T. Li, Y. Liu, S. Li, *J. Mater. Chem. B* **2017**, *5*, 7328.

[19] N. Urushihara, T. Hirai, A. Dager, Y. Nakamura, Y. Nishi, K. Inoue, R. Suzuki, M. Tanimura, K. Shinozaki, M. Tachibana, *ACS Appl. Nano Mater.* **2021**, *4*, 12472.

[20] Y. Shi, H. Xu, T. Yuan, T. Meng, H. Wu, J. Chang, H. Wang, X. Song, Y. Li, X. Li, Y. Zhang, W. Xie, L. Fan, *Aggregate* **2022**, *3*, e108.

[21] B. Zhao, Z. Tan, *Adv. Sci.* **2021**, *8*, 2001977.

[22] Z. Wang, N. Jiang, M. Liu, R. Zhang, F. Huang, D. Chen, *Small* **2021**, *17*, 2104551.

[23] H. Song, X. Liu, B. Wang, Z. Tang, S. Lu, *Sci. Bull.* **2019**, *64*, 1788.

[24] Z. Wang, F. Yuan, W. Sun, H. Shi, T. Hayat, A. Alsaedi, L. Fan, Z. Tan, *Adv. Opt. Mater.* **2019**, *7*, 1901299.

[25] C. Kang, S. Tao, F. Yang, B. Yang, *Aggregate* **2022**, *3*, e169.

[26] J. Ge, Q. Jia, W. Liu, L. Guo, Q. Liu, M. Lan, H. Zhang, X. Meng, P. Wang, *Adv. Mater.* **2015**, *27*, 4169.

[27] M. A. Pimenta, G. Dresselhaus, M. S. Dresselhaus, L. G. Cançado, A. Jorio, R. Saito, *Phys. Chem. Chem. Phys.* **2007**, *9*, 1276.

[28] a) Z. Wang, F. Yuan, X. Li, Y. Li, H. Zhong, L. Fan, S. Yang, *Adv. Mater.* **2017**, *29*, 1702910; b) C.-L. Shen, Q. Lou, C.-F. Lv, J.-H. Zang, S.-N. Qu, L. Dong, C.-X. Shan, *Adv. Sci.* **2019**, *6*, 1802331.

[29] G. Zheng, T. Wang, Q. Lou, C. Shen, M. Wu, J. Sun, W. Ji, J. Zang, K. Liu, L. Dong, C. Shan, *J. Phys. Chem. Lett.* **2022**, *13*, 1587.

[30] F. Qin, J. Bai, Y. Zhu, P. He, X. Wang, S. Wu, X. Yu, L. Ren, *Phys. Chem. Chem. Phys.* **2023**, *25*, 2762.

[31] Y. Shi, Z. Wang, T. Meng, T. Yuan, R. Ni, Y. Li, X. Li, Y. Zhang, Z. a. Tan, S. Lei, L. Fan, *J. Am. Chem. Soc.* **2021**, *143*, 18941.

[32] G. Huang, X. Chen, C. Wang, H. Zheng, Z. Huang, D. Chen, H. Xie, *RSC Adv.* **2017**, *7*, 47840.

[33] C. Shen, T. Jiang, Q. Lou, W. Zhao, C. Lv, G. Zheng, H. Liu, P. Li, L. Dai, K. Liu, J. Zang, F. Wang, L. Dong, S. Qu, Z. Cheng, C. Shan, *SmartMat* **2022**, *3*, 269.

[34] W. Liang, P. Wang, M. J. Meziani, L. Ge, L. Yang, A. K. Patel, S. O. Morgan, Y.-P. Sun, Nanoscale Advances 2021, 3, 4186; W. Liang, S. K. Sonkar, D. Saini, K. Sheriff, B. Singh, L. Yang, P. Wang, Y.-P. Sun, *Small*, DOI: 10.1002/smll.202206680.

[35] Y. Li, C. Liu, H. Sun, M. Chen, D. Hou, Y. Zheng, H. Xie, B. Zhou, X. Lin, *Adv. Sci.*, DOI: 10.1002/advs.202300543.

[36] W. Kwon, Y.-H. Kim, J.-H. Kim, T. Lee, S. Do, Y. Park, M. S. Jeong, T.-W. Lee, S.-W. Rhee, *Sci. Rep.* **2016**, *6*, 24205.

[37] F. Yuan, Y.-K. Wang, G. Sharma, Y. Dong, X. Zheng, P. Li, A. Johnston, G. Bappi, J. Z. Fan, H. Kung, B. Chen, M. I. Saidaminov, K. Singh, O. Voznyy, O. M. Bakr, Z.-H. Lu, E. H. Sargent, *Nat. Photonics* **2020**, *14*, 171.

[38] a) Q. Zhang, Y.-H. Song, J.-M. Hao, Y.-F. Lan, L.-Z. Feng, X.-C. Ru, J.-J. Wang, K.-H. Song, J.-N. Yang, T. Chen, H.-B. Yao, *J. Am. Chem. Soc.* **2022**, *144*, 8162; b) F. Shabani, H. Dehghanpour Baruj, I. Yurdakul, S. Delikanli, N. Gheshlaghi, F. Isik, B. Liu, Y. Altintas, B. Canımkurbey, H. V. Demir, *Small* **2022**, *18*, 2106115.

[39] Z. Wang, F. Wang, B. Zhao, S. Qu, T. Hayat, A. Alsaedi, L. Sui, K. Yuan, J. Zhang, Z. Wei, Z. Tan, *J. Phys. Chem. Lett.* **2020**, *11*, 1120.

[40] Q. Lou, Q. Ni, C. Niu, J. Wei, Z. Zhang, W. Shen, C. Shen, C. Qin, G. Zheng, K. Liu, J. Zang, L. Dong, C.-X. Shan, *Adv. Sci.* **2022**, *9*, 2203622.

[41] M. Liu, N. Jiang, H. Huang, J. Lin, F. Huang, Y. Zheng, D. Chen, *Chem. Eng. J.* **2021**, *413*, 127547.

[42] Q. Guo, X. Zhao, B. Song, J. Luo, J. Tang, *Adv. Mater.* **2022**, *34*, 2201008.

[43] Z. Chen, Z. Li, T. R. Hopper, A. A. Bakulin, H.-L. Yip, *Rep. Prog. Phys.* **2021**, *84*, 046401.

[44] T. Fang, T. Wang, X. Li, Y. Dong, S. Bai, J. Song, *Sci. Bull.* **2021**, *66*, 36.

[45] J. Zhao, C. Zheng, Y. Zhou, C. Li, J. Ye, X. Du, W. Li, Z. He, M. Zhang, H. Lin, S. Tao, X. Zhang, *Mater. Horiz.* **2019**, *6*, 1425.

[46] Q. Wang, Q.-S. Tian, Y.-L. Zhang, X. Tang, L.-S. Liao, *J. Mater. Chem. C* **2019**, *7*, 11329.

[47] X. Gong, S.-H. Lim, J. C. Ostrowski, D. Moses, C. J. Bardeen, G. C. Bazan, *J. Appl. Phys.* **2004**, *95*, 948.

Ultra-narrow-bandwidth deep-red electroluminescence based on green plant-derived carbon dots

ToC figure

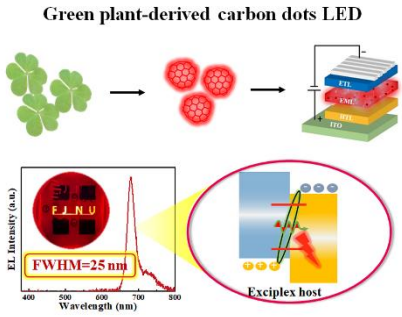

Bright deep-red fluorescent carbon dots (CDs) with an ultra-narrow FWHM of 21 nm and a high quantum yield of 52% are prepared by readily available green plants. High color-purity deep-red LEDs based on these CDs are demonstrated for the first time with Commission Internationale de l'Eclairage (CIE) coordinates of (0.692, 0.307) by using an exciplex host.